Translational Oncology 25 (2022) 101517

Contents lists available at ScienceDirect

Translational Oncology

journal homepage: www.elsevier.com/locate/tranon

Original Research

^{18}F-FDG Micro PET/CT imaging to evaluate the effect of BRCA1 knockdown on MDA-MB231 breast cancer cell radiosensitivity

Weitao Tao [a], Siqi Wang [b], Alei Xu [b], Yangyang Xue [b], Hui Wang [b], Huiqin Xu [a,b,*]

[a] School of Basic Medical Sciences, Anhui Medical University, No. 81 Meishan Road, Hefei 230032, China
[b] Department of Nuclear Medicine, The First Affiliated Hospital of Anhui Medical University, No. 218 Jixi Road, Hefei 230022, China

ARTICLE INFO

Keywords:
BRCA1
Breast cancer
Radiosensitivity
Fluorodeoxyglucose
PET/CT

ABSTRACT

Objective: Radioresistance of tumor cells is a major factor associated with failure of radiotherapy (RT). This study aimed to investigate the effect of BRCA1 knockdown on MDA-MB231 breast cancer cell radiosensitivity.
Materials and methods: Short hairpin RNA (shRNA) was used to knockdown BRCA1 gene in MDA-MB231 cells. Cell viability and proliferative capacity were assessed by CCK-8 and colony formation assays, respectively. We established xenograft models in nude mice to evaluate tumor volume and tumor weight. The mice were imaged by ^{18}F-fluorodeoxyglucose (^{18}F-FDG) positron emission tomography/computed tomography (PET/CT) before and after RT to evaluate changes in maximum standardized uptake value (SUV_{max}) and tumor SUV_{max}/muscle SUV_{max} (TMR). Changes in HIF-1α, Glut-1 and Ki-67 were analyzed and the correlation between ^{18}F-FDG uptake and tumor biology was analyzed.
Results: Compared with the control cells, RT significantly reduced cell viability and colony formation capacity in cells with the BRCA1 gene knockdown. In vivo assays showed that there was obvious delay in the tumor growth in the shBRCA1+RT group compared with the control group. ^{18}F-FDG Micro PET/CT indicated a reduction in glucose metabolism in the shBRCA1+RT group, with statistically significant differences in both the SUV_{max} and TMR. The data showed the expression of HIF-1α, Glut-1 and Ki-67 was downregulated in the shBRCA1+RT group, and both SUVmax and TMR had significant correlation with tumor biology.
Conclusion: These results demonstrated that BRCA1 knockdown improves the sensitivity of MDA-MB231 breast cancer cells to RT. In addition, ^{18}F-FDG PET/CT imaging allows non-invasive analysis of tumor biology and assessment of radiosensitivity.

Introduction

Breast cancer accounts for the highest cancer cases in the world, with an estimated 2.3 million cases per year and more than 680,000 deaths [1]. Breast cancer is the second most common cause of death in women, with women aged between 20 and 59 years being most affected [2]. Triple negative breast cancer (TNBC) is a subtype of breast cancer which lacks estrogen receptor (ER) or progesterone receptor (PR) and human epidermal growth factor receptor 2 (HER2) [3]. TNBC accounts for about 15% of all breast cancer patients and is highly aggressive, with a very poor prognosis and a five-year mortality rate of 40% [4,5]. Due to lack of specific molecular targets, there is no effective therapeutic option for TNBC.

Women with TNBC often undergo a combination of surgery, chemotherapy, RT and immunotherapy [6,7]. RT is one of the adjuvant treatment options administered following a breast cancer surgery. However, these systemic treatments have poor side effects, leading to higher recurrence rates and shorter overall survival [7,8]. Previous studies have shown that while tumor cells are damaged after receiving RT, the expression of relevant genes changes with changing environment and the tumor cells develop radioresistance. These events increase the incidence of cancer recurrence and metastatic disease, which ultimately lead to reduction or failure of the treatment [9–11].

BRCA1 as a breast cancer susceptibility gene, plays a critical role in DNA homologous recombination repair (HRR) with the RAD51 protein family [12,13]. At the occurrence of DNA damage, BRCA1 combines

Abbreviations: TNBC, Triple negative breast cancer; shRNA, Short hairpin RNA; ^{18}F-FDG, ^{18}F-fluorodeoxyglucose; PET/CT, Positron emission tomography/computed tomography; SUV_{max}, Maximum standardized uptake value; HRR, Homologous recombination repair.

* Corresponding author at: School of Basic Medical Sciences, Anhui Medical University, No. 81 Meishan Road, Hefei 230032, China.
E-mail address: hfhuiqinxu@163.com (H. Xu).

https://doi.org/10.1016/j.tranon.2022.101517
Received 8 June 2022; Received in revised form 29 July 2022; Accepted 9 August 2022

with BRCA1-associated RING domain protein 1 (BARD1) to form tumor suppressor complex BRCA1-BARD1, which recruits RAD51 and BRCA2-PALB2 (a tumor suppressor complex), into the vicinity of double-stranded DNA breaks [14–16]. Some studies have shown that BRCA1 knockdown can lead to significant reduction in HRR efficiency and has little effect on cell cycle distribution [17]. BRCA1 knockdown has also been shown to inhibit the formation of RAD51 foci in HRR-deficient tumor cells, thus halting the DNA repair program [18].

Tumor hypoxia and accelerated glycolysis are common in most malignant tumors and are associated with resistance to RT and chemotherapy [19,20]. The enhanced uptake and utilization of glucose in cancer is referred to as the Warburg effect [21]. ^{18}F-FDG is a radionuclide-labeled glucose analogue that can be used to monitor glucose metabolism in tumor tissues and is widely used in clinical practice. HIF-1α and Glut-1 are common tumor biomarkers, whose expression reflect the biological behavior of many malignant tumors. It has been shown that the expression of HIF-1α and Glut-1 is increased in RT-resistant breast cancer and other tumors, promoting tumor progression [22,23]. On the other hand, Ki-67 mediates the proliferation and invasion of tumor cells and thus can be a prognostic marker in tumor cells [24].

Therefore, since RT leads to DNA damage, silencing the BRCA1 gene does not support the repair the damage in breast cancer cells. We hypothesized that BRCA1 gene knockdown could increase the damage caused by RT and improve radiosensitivity in MDA-MB231 cells. Thus, we investigated the effect of silencing the BRCA1 gene in the response of MDA-MB-231 cell lines to RT and then employed ^{18}F-FDG Micro PET/CT imaging to monitor tumor glucose metabolism in nude mice models of breast cancer.

Materials and methods

Cell culture

Human breast cancer MDA-MB231 cell line was acquired from American Type Culture Collection (ATCC). The cell line was cultured in Dulbecco's modified Eagle's medium (DMEM; Gibco, USA), with a supplement of 10% fetal bovine serum (FBS; HyClone, USA), 5% penicillin/streptomycin (Gibco, USA) and placed in a 5% CO_2 incubator at 37 °C.

Lentivirus-mediated BRCA1 knockdown

Lentiviral shBRCA1 and a negative control lentiviral shRNA (shNC) were designed and synthesized by Hanbio (Shanghai, China). The target shRNA-BRCA1 sequence and the negative control sequence are shown in Table 1. According to the manufacturer's manual, MDA-MB231 cells were infected with the corresponding lentiviral shRNA at a multiplicity of infection with 20. The addition of 4 μg/ml polybrene to enhance the transfection efficiency. Stable shBRCA1 and shNC cells were selected for at least 3 generations with 2 μg/ml of puromycin.

RT-qPCR analysis

Total RNAs were extracted with Trizol reagent (Invitrogen, USA), and reverse transcribed into cDNA by using PrimeScript TMRT Master Mix kit (TaKaRa, Japan) according to the manufacturer's manual. RT-qPCR was performed using the SYBR Premix Ex TaqTM II kit (TaKaRa, Japan). Initial denaturation at 95 °C for 30 s, followed by 40 cycles of at 95 °C for 15 s and then 60 °C for 60 s. The cycle threshold (CT) value was defined as the number of PCR cycles in which the fluorescence signal exceeded the detection threshold value. The relative mRNA expression of targeting genes was analyzed by using the formula $2^{-\Delta\Delta CT}$. The pairs of primers are listed in Table 1.

Western blot analysis

Western blot was carried out according to standard methods, as described previously [25]. The primary antibodies used were: mouse anti-BRCA1 antibodies (Santa Cruz, USA), and mouse anti-GAPDH antibodies (Wanleibio, China). Anti-GAPDH antibodies expression was used as loading control. The secondary antibody was Sheep anti-rabbit IgG-HRP (Wanleibio, China). Quantitative analysis of protein expression was performed using Image J software (National Institutes of Health, USA).

CCK-8 assay

The CCK-8 assay was used to assess the cell viability and proliferation. Cells were seeded in 96-well plates at a density of 1×10^3 cells/well. One day later, the cells were received to 4 Gray (Gy) of radiation. Then CCK-8 reagent (Beyotime, Shanghai, China) was then added to the cell culture medium daily for three days. One hour after CCK-8 addition, the absorbance was measured at a wavelength of 490 nm by a microplate reader (BioTek Instruments, USA). The experiments were independently performed for three times.

Colony formation assay

The cells were seeded in 6-well plates with a density of 500 cells/well. After overnight culture, the cells were exposed to 0, 2, 4, 6 and 8 Gy X-rays at a dose rate of 4 Gy/min. Thereafter, the cells were cultured in a 37 °C incubator for 2 weeks. The colonies were fixed with 4% paraformaldehyde for 30–40 min and then stained with 0.5% crystal violet for 30 min. Colonies with more than 50 cells stained were counted using the Image J software and then survival fraction (SF) was calculated. The cell survival curves were fitted according to the multi-target single-hit model ($SF = 1 - (1 - \exp(-D/D_0))^N$) and survival enhancement rate (SER) was calculated by acquiring some radiobiological parameters, such as K, N, D_0, D_q and D_{37}. where D is the irradiation dose, K is the

Table 1
Primers used in plasmid construction and RT-qPCR.

Name		Sequence (5′−3′)
shNC	Fw	GATCCGTTCTCCGAACGTGTCACGTAATTCAAGAGATTACGTGACACGTTCGGAGAATTTTTTC
	Rw	AATTGAAAAAATTCTCCGAACGTGTCACGTAATCTCTTGAATTACGTGACACGTTCGGAGAACG
shBRCA1	Fw	GATCCGCAGCAGAGGGATACCATGCAACATACTCGAGTATGTTGCATGGTATCCCTCTGCTGTTTTTTG
	Rw	AATTCAAAAAACAGCAGAGGGATACCATGCAACATACTCGAGTATGTTGCATGGTATCCCTCTGCTGCG
BRCA1	qFw	GAACGGGCTTGGAAGAAAAT
	qRw	GTTTCACTCTCACACCCAGA
GAPDH	qFw	ACAGTCAGCCGCATCTTCTT
	qRw	GACAAGCTTCCCGTTCTCAG

Fw: forward primer. Rw: reverse primer. qFw: forward primer for RT-qPCR. qRw: reverse primer for RT-qPCR.

passivation constant of the cell survival curve, N is the value of the point where the linear portion of the curve extends and intersects the vertical axis (both K and N can be obtained directly from the fitted curves). D_0 represents the average lethal dose ($D_0 = 1/K$), which is the theoretical amount of radiation energy required to make an average of one hit per cell. D_q means quasithreshold dose which represents the width of the curve shoulder ($D_q = D_0 \times \ln N$), and characterizes the ability to repair sublethal damage. D_{37} is the corresponding radiation dose at a cell survival fraction of 37% ($D_{37} = D_0 + D_q$). The SER_{37} equation is as follows: SER_{37} = negative control group D_0/silencing group D_0.

Xenograft tumor model and treatment

Four-to five-week-old female BALB/c nude mice (20–25 g), were provided by Beijing Vital River Laboratory Animal Technology. The mice were housed in an environment with a temperature of 26 ± 1 °C relative humidity of 50 ± 1%, and a light/dark cycle of 12/12 h. All the animal experiments were approved by the Ethics Review Committee for Animal Experimentation of Anhui Medical University (No. LLSC20211059). Nude mice were anesthetized with 1% isoflurane-to-air mixture and then injected with 5.0×10^6 MDA-MB231 cells in the right upper limb armpit region. Tumors > 10 mm in vernier caliper were selected for subsequent experiments. The nude mice were randomly divided into four groups ($n = 6$/group): shNC group; shNC+RT group; shBRCA1 group and shBRCA1+RT group. Nude mice receiving RT were irradiated with VARIAN 23 EX medical linear accelerator (Varian Medical System Inc, Palo Alto CA, USA) every other day for one week at a dose of 4 Gy, 4 Gy/min, as shown in Fig. 1.

Assessment of tumor volume and tumor weight

The tumor diameters started to be measured when the tumor shapes could be observed. Tumor diameters were measured by vernier caliper once every two days and tumor volume (V) was calculated as [V = length (cm) × width^2 (cm^2) × π/6]. After the last PET/CT imaging, the animals were euthanized and the tumors were separated and weighed.

^{18}F-FDG Micro PET/CT imaging and analysis

Each mouse was scanned using ^{18}F-FDG Micro PET/CT (Siemens, Germany, Small-Animal PET research center of Shanghai Ruijin Hospital) before RT and 24 h after the last RT. The radiochemical purities of ^{18}F-FDG were more than 95%. Each mouse received 5.55 MBq (150μCi) of ^{18}F-FDG through a tail vein injection 60 min before the start of the scan. Isoflurane (1% isoflurane-to-air mixture) was administered before the scan. PET images were reconstructed using the Inveon Acquisition Workplace software (version 2.0, Siemens Preclinical Solutions). On the other hand, the SUV_{max} was determined by measuring the maximal concentration of radioactivity in the region of interest (ROI) for semi-quantitative evaluation of ^{18}F-FDG uptake in tumors. The SUV_{max} within ROI was calculated using the following formula: concentration of radioactivity in the ROI (MBq/mL) × total body weight (kg)/injected radioactivity (g/MBq). The PET/CT metric for statistical analysis was determined as the tumor tissue SUVmax (T), the contralateral normal muscle SUV_{max} (M), and the ratio of the two values (TMR).

Pathological assays

The tumors were harvested and fixed in 4% paraformaldehyde, and then tumor samples were removed and embedded in paraffin. For Hematoxylin and Eosin and immunohistochemical staining, the sections were cut into sections measuring 4 μm in thickness. The tissue sections were then incubated with anti-HIF-1a antibodies (dilution: 1:200, Beyotime Biotechnology, Shanghai, China), anti-Glut-1 antibodies (dilution: 1:300, Beyotime Biotechnology, Shanghai, China) or anti-Ki-67 antibodies (dilution: 1:200, Beyotime Biotechnology, Shanghai, China), followed by horseradish peroxidase–conjugated antirabbit IgG (dilution: 1:200; Beyotime Biotechnology, Shanghai, China). Thereafter, DAB chromogenic kit (Beyotime Biotechnology, Shanghai, China) was used to stain and visualize the positive cells.

The data were analyzed using the Image-Pro-Plus 6.0 software (Media Cybernetics, USA). The integrated optical density (IOD) was employed to evaluate the area and intensity of the positive staining. The IOD of all positive stains was obtained from selected areas in each section, and the results were expressed as mean density = Sum (IOD)/Sum (Area). All the section under immunohistochemical staining were assessed by at least two observers.

Statistical analysis

All data were expressed as mean ± standard deviation (SD). Statistical analysis was performed using SPSS 26.0 (Armonk, USA) and GraphPad Prism 8.3 Software (San Diego, USA). The comparison between two groups was analyzed by independent-samples t-test or paired-sample t-test, the comparison among multiple groups was analyzed by one-way ANOVA analysis and with the LSD post hoc test. The association of ^{18}F-FDG uptake with HIF-1a, Glut-1 and Ki-67 were assessed by Pearson correlation analysis. P value < 0.05 was considered statistically significant.

Results

Lentivirus-mediated BRCA1 knockdown in MDA-MB231 cells

We successfully generated stable BRCA1 knockdown MDA-MB231 breast cancer cells using a lentivirus-mediated system. Our western blot and RT-qPCR analyses showed that the levels of BRCA1 protein and mRNA expression were significantly lower in the BRCA1 knockdown

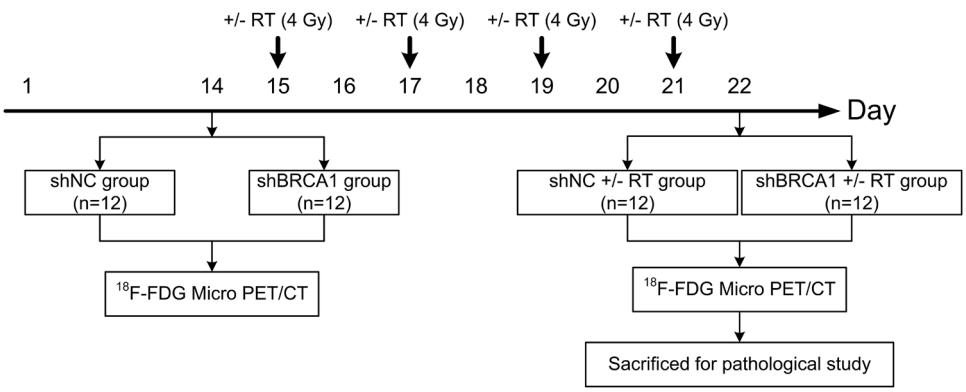

Fig. 1. Outline of tumor implantation, RT, and imaging schedule (Day 1 is the tumor cells implantation day).

cells compared with matched shNC group cells (both $P < 0.001$) (Fig. 2A-C).

Effects of silencing BRCA1 on proliferation in vitro

The effects of RT on cell proliferation capacity and viability in the BRCA1 knock down cells were examined by the CCK-8 and colony formation assays. As shown in Fig. 2D-G, RT reduced cell viability and

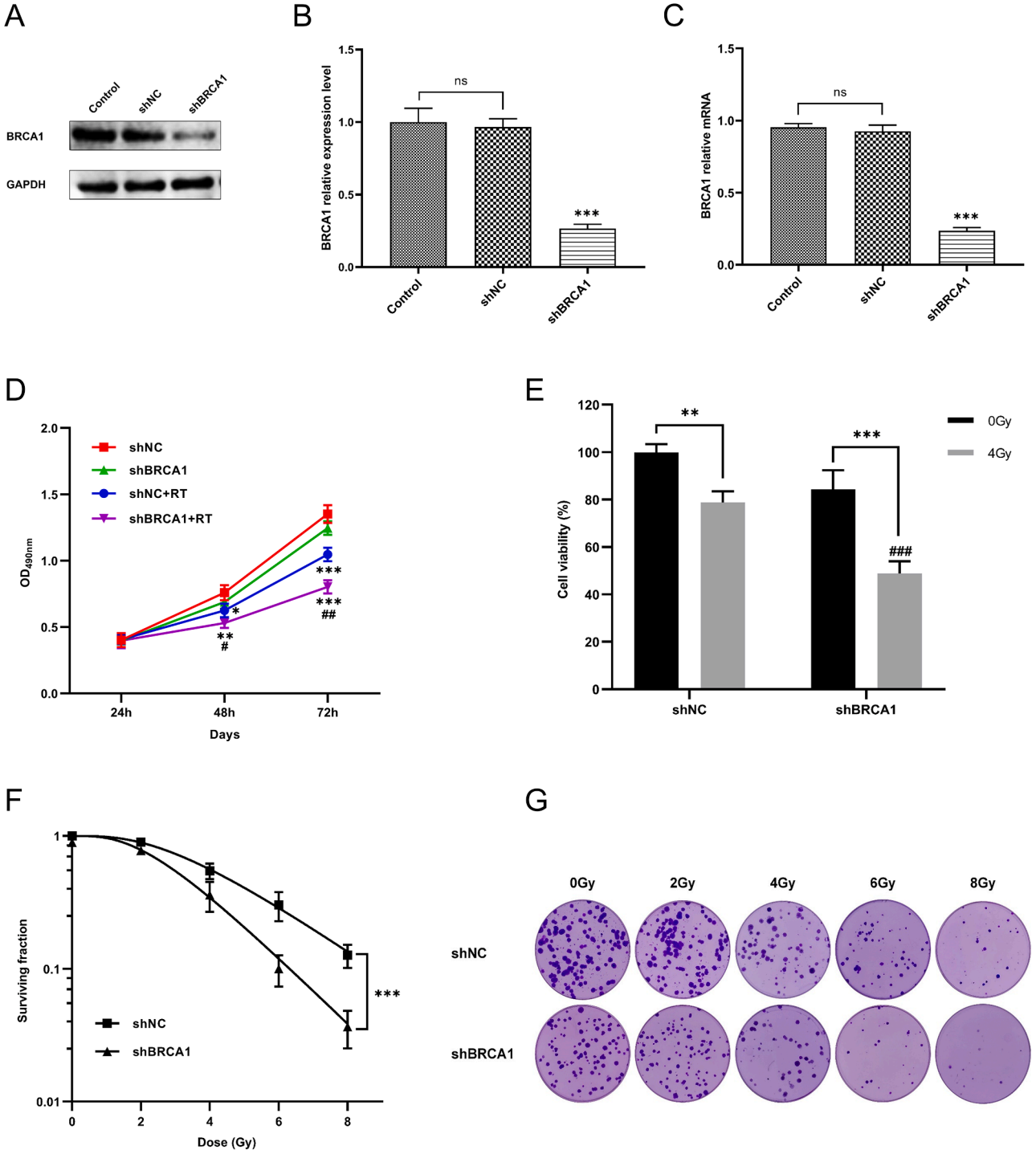

Fig. 2. Effect of silencing BRCA1 gene on cell viability and proliferation in vitro experiments. Control group: no transduction; shNC group: breast cell lines stably transduced with negative control lentiviral shRNA; shBRCA1 group: breast cell lines stably transduced with lentivirus-mediated BRCA1 shRNA. (A) BRCA1 protein expression was analyzed by western blotting with GAPDH as a control. (B) Western blotting results of the three groups of cells were represented by quantitative graphs. (C) BRCA1 mRNA was determined by RT-qPCR. (D) Changes in OD_{490nm} values of cells in shNC and shBRCA1 group at 24 h, 48 h and 72 h after 4 Gy irradiation. (E) Cell viability of cells in shNC and shBRCA1 group at 48 h after 0 or 4 Gy irradiation. (F) Survival curve was fitted according to the multi-target single-hit model. (G) Representative images of respective colony formation in two groups of cells at different doses (0, 2, 4, 6, and 8 Gy). Data are shown as mean ± standard deviation (SD) from three independent experiments. $^{*}P < 0.05$, $^{**}P < 0.01$, $^{***}P < 0.001$, vs. shNC group or shBRCA1 group; $^{\#\#}P < 0.01$, $^{\#\#\#}P < 0.001$ vs. shNC + RT group.

colony formation in both groups. Although the cell viability and colony formation were inhibited in the shNC cells after RT, there was significant inhibition in the cells with silenced BRCA1 gene (both $P < 0.001$). We then calculated the radiobiological parameters in the two groups by multi-target single-hit model. Both shNC and shBRCA1 cells had a D_0 of 2.42 and 1.72, respectively; where the D_0 value represents the average radiation lethal dose, which can be used as an indicator of cell radiosensitivity. The SER_{37} in the shBRCA1 cells was equal to 1.41. Other radiobiological parameters were shown in Table 2.

^{18}F-FDG Micro PET/CT imaging

^{18}F-FDG Micro PET/CT imaging was performed for each group of nude mice before and 24 h after treatment (Fig. 3A). In this experiment, we analyzed the SUV_{max} and TMR values of the tumor tissues as shown in Table 3. The data showed that there was no significant difference in the ^{18}F-FDG uptake of tumor tissues before treatment among the four groups ($F = 0.039$, $P > 0.05$; $F = 1.354$, $P > 0.05$). However, there was a significant difference in the ^{18}F-FDG uptake of tumor tissues after treatment among the four groups ($F = 17.492$, $P < 0.05$; $F = 89.982$, $P < 0.05$). Comparison of the ^{18}F-FDG uptake in the tumor tissues after treatment revealed that the shBRCA1 + RT group had lower SUV_{max} and TMR values compared with those in the shNC + RT group ($P < 0.05$; $P < 0.01$) (Fig. 3B). In addition, the growth rate of the tumor tissue SUV_{max} was shown to be 25.50%, −26.97%, 22.82% and −54.42% for each group.

BRAC1 knockdown compared with RT delay tumor growth

As shown in Fig. 3C, there was slow increase in tumor volume in the RT group, while there was significant increase in tumor volume in the group that did not receive RT. In addition, there was slower tumor growth in the BRCA1-silenced cells compared to the shNC cells, especially at day 22 after cell implantation ($P < 0.001$). Similar trend was found in the tumor weight differences (Fig. 3D). These results showed that RT reduced the tumor sizes and weight compared to those without RT. Furthermore, tumor size and weight were significantly smaller in the shBRCA1 + RT group than in the shNC + RT group ($P < 0.001$).

Pathological analysis

Our analysis showed that the fresh tumor tissues were bright red, with gray necrotic areas in some of the tumors. As shown in Fig. 4A, Hematoxylin and Eosin and immunohistochemical staining showed that the tumor cells had large cell nuclear with darker staining and obvious heterogeneity. Unlike in the groups which did not undergo RT which had higher number of cells, there was reduction in the number of cells with necrotic areas in the groups that received RT. In addition, shBRCA1 + RT group had the least number of cells and more necrotic areas. Immunohistochemical analysis showed that HIF-1α, Glut-1 and Ki-67 were highly expressed in tumor tissues, and the mean density of HIF-1α, Glut-1 and Ki-67 was significantly suppressed in both groups receiving RT. In the shBRCA1 + RT group, the mean density of HIF-1α, Glut-1 and Ki-67 was significantly lower compared with the other groups (Fig. 4B). Our correlation analysis demonstrated that tumor tissue SUV_{max} was significantly correlated with HIF-1α, Glut-1 and Ki-67 expression ($r = 0.804$; $r = 0.774$; $r = 0.687$, all $P < 0.01$) (Fig. 5A). Similarly, the TMR values were also significantly correlated with HIF-1α, Glut-1 and Ki-67 expression ($r = 0.883$; $r = 0.802$; $r = 0.822$, all $P < 0.01$) (Fig. 5B).

Table 2
Summary of radiobiological parameters.

Group	K	N	D_0	D_q	D_{37}	SER_{37}
shNC	0.41	3.86	2.42	3.27	5.69	–
shBRCA1	0.58	4.09	1.72	2.42	4.14	**1.41**

K is the passivation constant of the cell survival curve.
N is the value of the point where the linear portion of the curve extends and intersects the vertical axis.
D_0 represents the average lethal dose ($D_0 = 1/K$), it's the theoretical amount of radiation energy required to make an average of one hit per cell.
D_q means quasithreshold dose represents the width of the curve shoulder ($D_q = D_0 \times \ln N$), which characterizes the ability to repair sublethal damage.
D_{37} means dose [Gy] to reduce survival fraction to 37% ($D_{37} = D_0 + D_q$).
$SER_{37} = D_0$ (shNC)/D_0 (shBRCA1). The SER greater than 1.20 indicate radiosensitization.

Discussion

RT is an essential treatment option for breast cancer, which has been shown to reduce the rate of recurrence and the risk of death. Adjuvant RT after breast-conserving surgery, or in early-stage breast cancer and lymphatic involvement has been widely accepted for breast cancer treatment [26,27]. However, there are still many patients who are threatened with relapse and even death. In many tumor types, recurrence has been associated with acquired radioresistance [28]. A previous randomized clinical trial showed that RT did not reduce death from any reason in any breast cancer subtype [29]. Thus, radioresistance presents a formidable clinical challenge in the systematic treatment of breast cancer. Many studies have extensively evaluated many genes that are associated with tumor radiosensitivity. For example, the role of the apoptosis gene BTG1 [30], HRR gene RAD51 [31] and cell hypoxia-associated gene HIF-1α in radiosensitivity has been defined [32]. However, the role of BRCA1 in response to radiation therapy in breast cancer is poorly understood. Therefore, we investigated the relationship between BRCA1 and radiosensitivity, which is a critical gene in the HRR process. In this study, shRNA-BRCA1 was introduced into the MDA-MB231 cells with the help of lentivirus vector, and was successfully integrated into the genome of the MDA-MB231 cells after infection, thus achieving stable and long term expression.

Our CCK-8 assay demonstrated that the BRCA1 knockdown significantly reduced cell viability after irradiation with 4 Gy and the cell viability was still poor at 48 h and 72 h after RT. In the colony formation assay, we showed that the cell survival rate of the shBRCA1 group was significantly lower than that of the shNC group. BRCA1 gene knockdown suppressed the colony formation in the MDA-MB231 cells with a SER_{37} of 1.41. These data show that BRCA1 gene knockdown increased the sensitivity of the MDA-MB231 cells to RT. In summary, RT had a higher effect in inhibiting cell proliferation and promoting cell death in BRCA1 knockdown cells with, indicating that BRCA1 knockdown can enhance the sensitivity of tumor cells to radiation.

Previous evidence showed that BRCA1, a major breast cancer suppressor gene, plays an important role in regulating genome stability and DNA repair based on HRR as well as in the repair of DNA double-strand breaks to maintain the fidelity of the genome [33,34]. Yinghua Zhu et al. demonstrated that reduction of the BRCA1 expression with PI3K inhibitors restored tamoxifen resistance and sensitivity to cisplatin in breast cancer cells [35]. The use of PARP inhibitors and cisplatin has been shown to prolong overall survival and progression-free survival in breast cancer patients with BRCA1/2-mutated or HRR-deficiency [36, 37]. In this study, we successfully silenced BRCA1 gene expression using a lentiviral shRNA approach in MDA-MB231 cells, making the cells to produce HRR-deficiency. Radiation causes DNA strand damage in tumors, and BRCA1 knockdown can inhibit the DNA damage repair process by a series of DNA repair proteins. This suggests that silencing BRCA1 gene plays a role in radiosensitization of tumor cells.

Hypoxia is a typical feature in most solid tumors [38]. Hypoxia and increased HIF-1α activity within the tumor are associated with tumor recurrence and distant metastasis, as well as poor prognosis after radiotherapy. In the early stages of tumor formation, the tumor is often in a hypoxic environment due to the rapid rate of angiogenesis, which stimulates the release of HIFs. The hypoxic microenvironment of solid

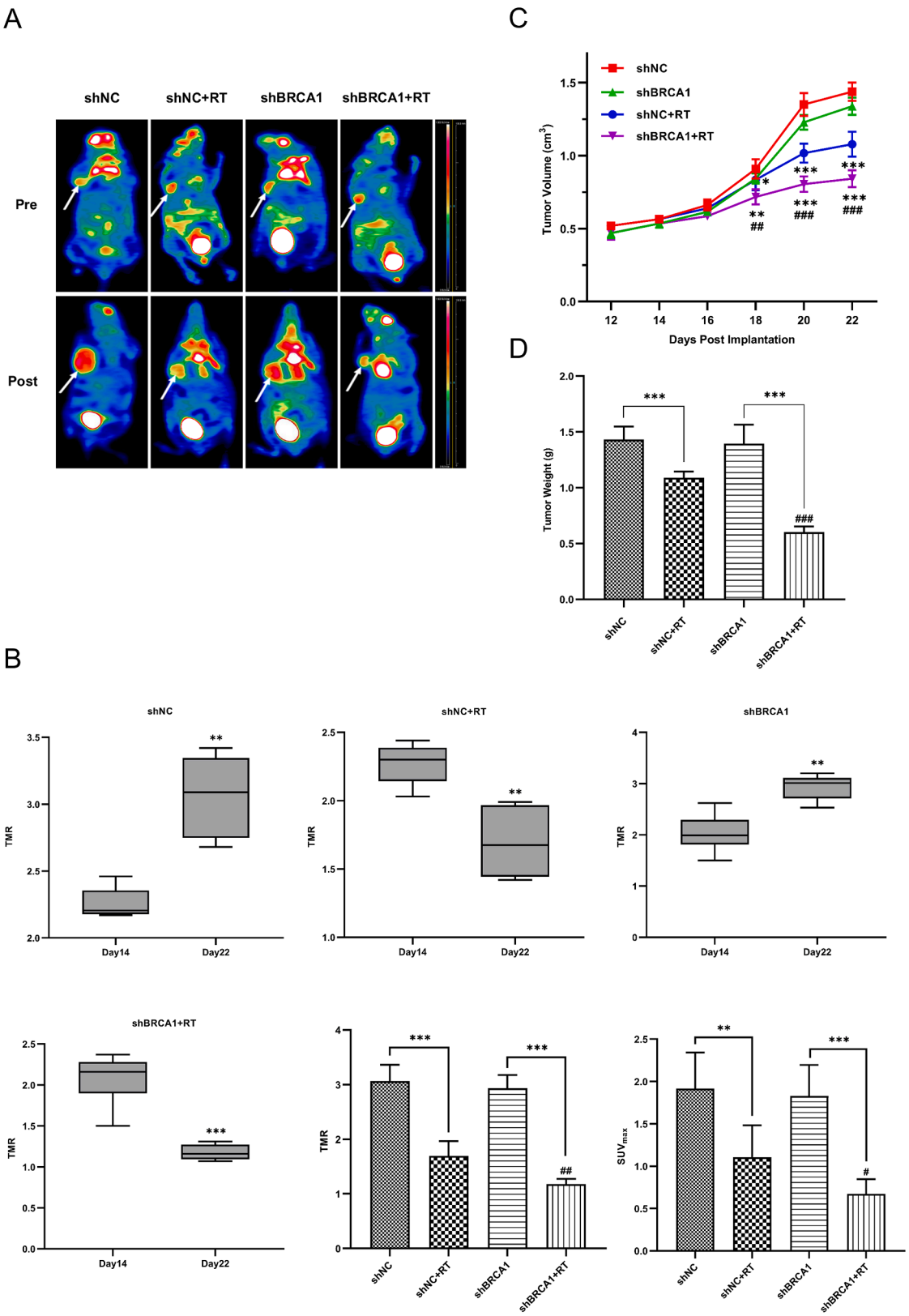

Fig. 3. ^{18}F-FDG Micro PET/CT imaging of tumor xenografts from BALB/c nude mice treated with RT. The BALB/c nude mice were randomly divided into four groups (n = 6/group). (A) Representative coronal ^{18}F-FDG Micro PET/CT images of tumors from different groups of mice at day 14 and day 22. Tumors are indicated by white arrows. (B) Tumor volume (cm^3) was assessed every 2 days. (C) Tumor weight (g) was assessed for different groups of mice after 4 times RT. (D) Quantification of SUV_{max} and TMR values of tumors from different groups of mice. Data are shown as mean ± SD (n = 6/group). $^{*}P < 0.05$, $^{**}P < 0.01$, $^{***}P < 0.001$, vs. shNC group, shBRCA1 group or day 14; $^{\#}P < 0.05$, $^{\#\#}P < 0.01$, $^{\#\#\#}P < 0.001$ vs. shNC + RT group.

Table 3
Changes in SUV_{max} and TMR by ^{18}F-FDG Micro PET/CT imaging.

	SUV_{max}			TMR		
	Pre-RT	Post-RT	*P*-value	Pre-RT	Post-RT	*P*-value
shNC	1.53 ± 0.40	1.92 ± 0.43	*P* = 0.019	2.26 ± 0.11	3.06 ± 0.30	*P* = 0.001
shNC+RT	1.52 ± 0.22	1.11 ± 0.37	*P* = 0.002	2.27 ± 0.15	1.70 ± 0.27	*P* = 0.008
shBRCA1	1.49 ± 0.37	1.83 ± 0.37	*P* = 0.003	2.03 ± 0.37	2.93 ± 0.24	*P* = 0.008
shBRCA1+RT	1.47 ± 0.38	0.67 ± 0.18	*P* = 0.005	2.08 ± 0.31	1.18 ± 0.10	*P* < 0.001

tumors reduces the sensitivity of the tumor to chemo-radiotherapy, thus increasing the risk of tumor recurrence and metastasis [39]. HIF-1α promotes the growth of endothelial cells after radiotherapy by inducing the expression of crucial downstream genes, which include Glut-1, and thus promoting tumor resistance to radiotherapy. Ki-67, is a marker of cell proliferation, and is important in evaluating the prognosis of early-stage breast cancer, guiding chemotherapy, predicting the effect of chemotherapy, and in neoadjuvant chemotherapy. This study showed that the use of RT in BRCA1 knockdown cells significantly improves the tumor hypoxic microenvironment by downregulating the expression level of HIF-1α, Glut-1 and Ki-67 genes.

^{18}F-FDG is a common imaging agent used to detect the degree of aggressiveness of malignant tumors. The ^{18}F-FDG PET/CT imaging, as a radionuclide imaging technique, has been widely used in the clinic and

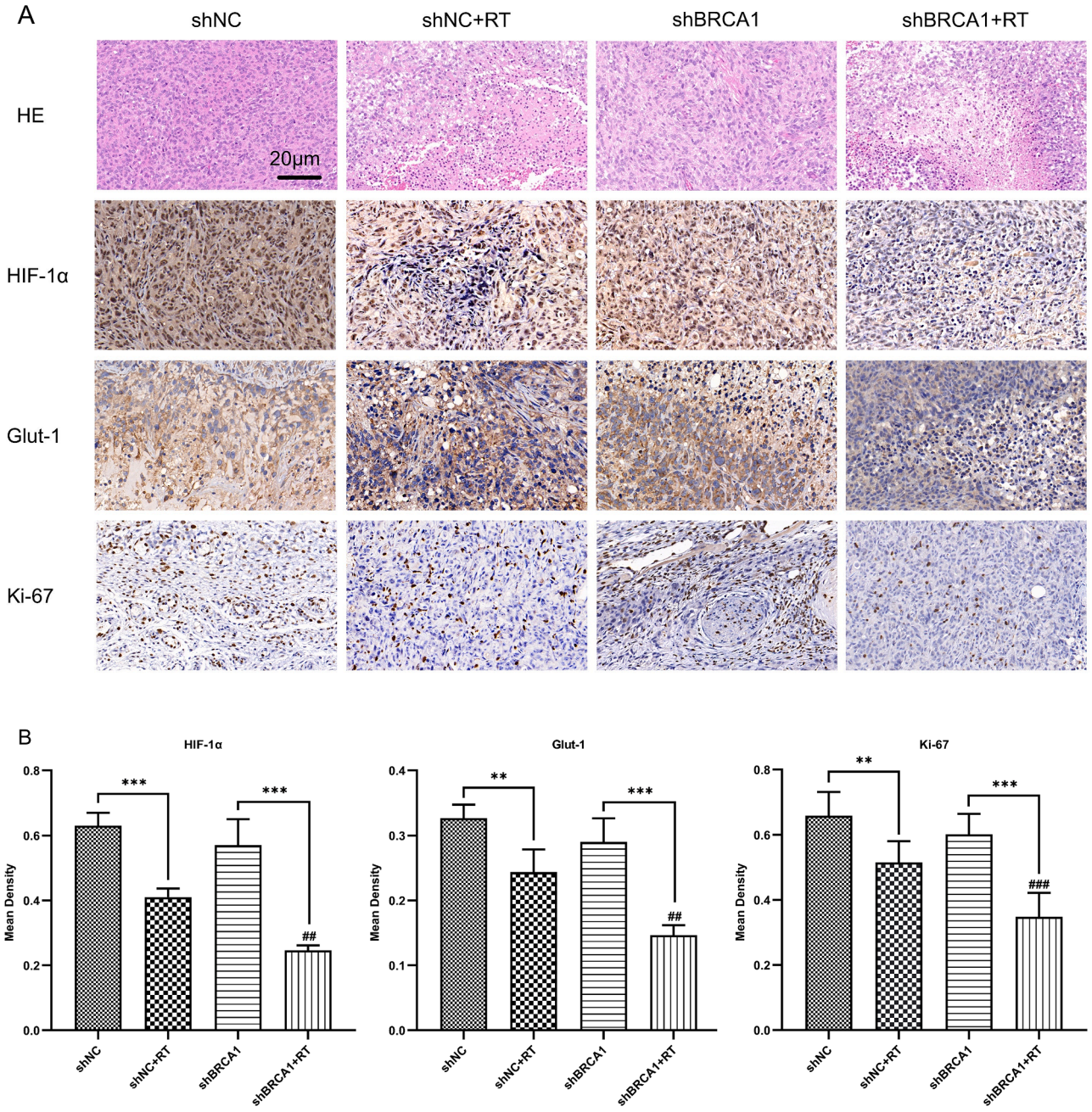

Fig. 4. The effect of knockdown of BRCA1 gene combined with RT on tumor biomarkers. (A) Pathological analysis the Hematoxylin and Eosin staining and the expression of HIF-1α, Glut-1 and Ki-67 in tumors (magnification = 40 ×). (B) Quantification of immunohistochemical analysis using mean density. Data are shown as mean ± SD (n = 6/group). $^{**}P < 0.01$, $^{***}P < 0.001$, vs. shNC group or shBRCA1 group; $^{\#\#}P < 0.01$, $^{\#\#\#}P < 0.001$ vs. shNC + RT group.

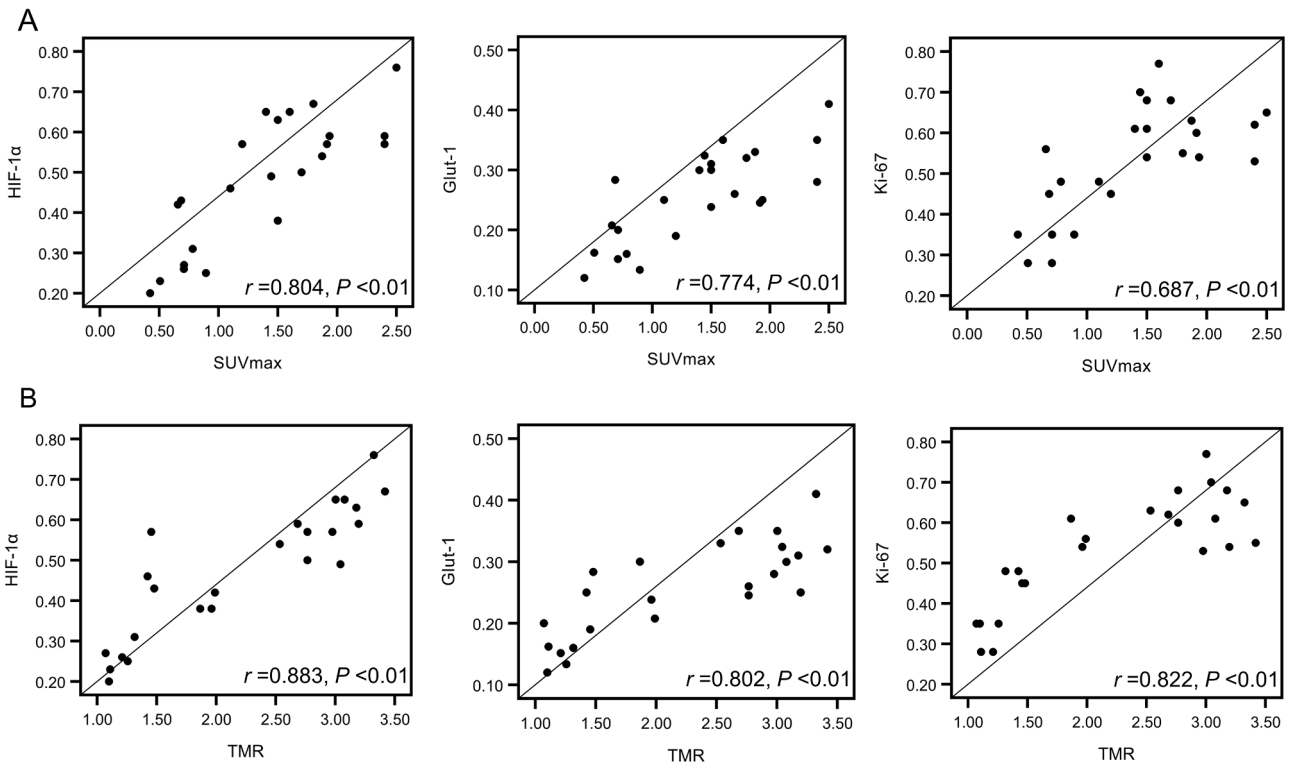

Fig. 5. Correlation analysis between ^{18}F-FDG uptake and tumor biomarkers. (A) Correlation between SUV_{max} and the expression of HIF-1α, Glut-1 and Ki-67. (B) Correlation between TMR and the expression of HIF-1α, Glut-1 and Ki-67.

research. A previous meta-analysis [40] showed a significant effect of ^{18}F-FDG PET/CT on the staging and treatment of breast cancer patients, resulting in benefits from locally aggressive therapies and prolonged survival. Both SUV_{max} and TMR can be used as prognostic factors in various malignancies, and a previous study [41] has showed a significant correlation between high SUV_{max} and poor prognosis in breast cancer patients. Indeed, this is the first study to use ^{18}F-FDG Micro PET/CT imaging to evaluate tumor growth metabolism after RT in nude mice model of BRCA1-silenced breast cancer cells. In the vivo experiments, we generated a mice model of breast cancer by injecting cells in the right upper limb armpit region of nude mice. This was because of the nature of the imaging readout, which did not choose a more appropriate orthotopic method. The PET/CT imaging results showed that tumors that did not receive RT had higher ^{18}F-FDG uptake on day 22, while the uptake was reduced to different degrees in those groups which underwent RT. TMR and SUV_{max} were particularly reduced in the shBRCA1 + RT group, a finding consistent with the low expression of HIF-1α, Glut-1 and Ki-67. These data show that the use of RT in cells with BRCA1 knockdown significantly improved glucose metabolism in breast tumors. Besides, this data was in sync with the findings that this group had slower tumor volume growth and had lighter tumor weight. The expression of HIF-1α, Glut-1 and Ki-67 correlated significantly with the ^{18}F-FDG uptake, which agreed with the findings of Bravatà et al. [42–44]. Together, these results suggested that RT can largely inhibit the growth of tumor tissues with a radiosensitizing effect in BRCA1 knockdown group, and this change can be dynamically monitored and assessed by the ^{18}F-FDG PET/CT imaging.

These findings may not only provide new research direction to overcome breast cancer radioresistance, but also that BRCA1 may be a new therapeutic target for TNBC by increasing the sensitivity to RT. Several studies [45–48] have demonstrated the value of gene therapy combined with nuclear medicine imaging in tumor imaging and treatment. However, further researches need to be explored in the future about how to prepare a novel positron emitter-labeled short interfering (siRNA) or shRNA, and real-time analysis of siRNA or shRNA trafficking was performed by using PET imaging to provide new approaches for clinical breast cancer imaging, diagnosis, and treatment.

We have some limitations on this study. For example, we didn't investigate the effect of RT on BRCA1 knockdown breast cancer cells at a more molecular level. Some studies on protein expression during HRR and signaling pathways. In this study, only one type of TNBC cell line was used, and the effects of radiosensitivity on other breast cancer cell lines need to be studied to confirm our experimental results. Further research is needed to confirm the findings and define molecular mechanisms underlying the effect of RT on BRCA1 knockdown breast cancer cells.

Conclusion

Overall, our analyses demonstrate that BRCA1 gene knockdown enhances the radiosensitivity of MDA-MB231 breast cancer cells and can downregulate multiple biomarkers of poor prognosis, which may be a novel approach to be used in improving the efficacy of RT. ^{18}F-FDG PET/CT imaging allows non-invasive acquisition of tumor biology and radiosensitization response assessment.

CRediT authorship contribution statement

Weitao Tao: Conceptualization, Methodology, Writing – original draft. **Siqi Wang:** Software, Data curation. **Alei Xu:** Software, Data curation. **Yangyang Xue:** Software, Data curation, Visualization. **Hui Wang:** Writing – review & editing. **Huiqin Xu:** Writing – review & editing.

Declaration of Competing Interest

The authors declare that they have no known competing financial interests or personal relationships that could have appeared to influence the work reported in this paper.

Acknowledgments

We are grateful to the Department of Nuclear Medicine of Ruijin Hospital affiliated to Shanghai Jiaotong University for providing laboratory support, Micro PET/CT and ^{18}F-FDG for animal imaging. This work was supported by the National Natural Science Foundation of China (No. 81971643).

Supplementary materials

Supplementary material associated with this article can be found, in the online version, at doi:10.1016/j.tranon.2022.101517.

References

[1] H. Sung, J. Ferlay, R.L. Siegel, M. Laversanne, I. Soerjomataram, A. Jemal, F. Bray, Global cancer statistics 2020: GLOBOCAN estimates of incidence and mortality worldwide for 36 cancers in 185 countries, CA Cancer J. Clin. 71 (3) (2021) 209–249.
[2] R.L. Siegel, K.D. Miller, H.E. Fuchs, A. Jemal, Cancer statistics, 2021, CA Cancer J. Clin. 71 (1) (2021) 7–33.
[3] G. Bianchini, J.M. Balko, I.A. Mayer, M.E. Sanders, L. Gianni, Triple-negative breast cancer: challenges and opportunities of a heterogeneous disease, Nat. Rev. Clin. Oncol. 13 (11) (2016) 674–690.
[4] A.G. Waks, E.P. Winer, Breast cancer treatment: a review, JAMA 321 (3) (2019) 288–300.
[5] C. Denkert, C. Liedtke, A. Tutt, G. von Minckwitz, Molecular alterations in triple-negative breast cancer—the road to new treatment strategies, Lancet 389 (10087) (2017) 2430–2442.
[6] J.M. Lebert, R. Lester, E. Powell, M. Seal, J. McCarthy, Advances in the systemic treatment of triple-negative breast cancer, Curr. Oncol. 25 (Suppl 1) (2018) S142–S150.
[7] S. Al-Mahmood, J. Sapiezynski, O.B. Garbuzenko, T. Minko, Metastatic and triple-negative breast cancer: challenges and treatment options, Drug Deliv. Transl. Res. 8 (5) (2018) 1483–1507.
[8] A. Lee, M.B.A. Djamgoz, Triple negative breast cancer: emerging therapeutic modalities and novel combination therapies, Cancer Treat. Rev. 62 (2018) 110–122.
[9] A.E.M. Post, M. Smid, A. Nagelkerke, J.W.M. Martens, J. Bussink, F. Sweep, P. N. Span, Interferon-stimulated genes are involved in cross-resistance to radiotherapy in tamoxifen-resistant breast cancer, Clin. Cancer Res. 24 (14) (2018) 3397–3408.
[10] D. Candas-Green, B. Xie, J. Huang, M. Fan, A. Wang, C. Menaa, Y. Zhang, L. Zhang, D. Jing, S. Azghadi, W. Zhou, L. Liu, N. Jiang, T. Li, T. Gao, C. Sweeney, R. Shen, T. Y. Lin, C.X. Pan, O.M. Ozpiskin, G. Woloschak, D.J. Grdina, A.T. Vaughan, J. M. Wang, S. Xia, A.M. Monjazeb, W.J. Murphy, L.Q. Sun, H.W. Chen, K.S. Lam, R. R. Weichselbaum, J.J. Li, Dual blockade of CD47 and HER2 eliminates radioresistant breast cancer cells, Nat. Commun. 11 (1) (2020) 4591.
[11] L. Lu, J. Dong, L. Wang, Q. Xia, D. Zhang, H. Kim, T. Yin, S. Fan, Q. Shen, Activation of STAT3 and Bcl-2 and reduction of reactive oxygen species (ROS) promote radioresistance in breast cancer and overcome of radioresistance with niclosamide, Oncogene 37 (39) (2018) 5292–5304.
[12] W. Sieh, J.H. Rothstein, R.J. Klein, S.E. Alexeeff, L.C. Sakoda, E. Jorgenson, R. B. McBride, R.E. Graff, V. McGuire, N. Achacoso, L. Acton, R.Y. Liang, J.A. Lipson, D.L. Rubin, M.J. Yaffe, D.F. Easton, C. Schaefer, N. Risch, A.S. Whittemore, L. A. Habel, Identification of 31 loci for mammographic density phenotypes and their associations with breast cancer risk, Nat. Commun. 11 (1) (2020) 5116.
[13] D. Cortez, Replication-coupled DNA repair, Mol. Cell 74 (5) (2019) 866–876.
[14] M. Suszynska, W. Kluzniak, D. Wokolorczyk, A. Jakubowska, T. Huzarski, J. Gronwald, T. Debniak, M. Szwiec, M. Ratajska, K. Klonowska, S. Narod, N. Bogdanova, T. Dork, J. Lubinski, C. Cybulski, P. Kozlowski, BARD1 is a low/moderate breast cancer risk gene: evidence based on an association study of the Central European p.Q564X recurrent mutation, Cancers (Basel) 11 (6) (2019).
[15] M. Tarsounas, P. Sung, The antitumorigenic roles of BRCA1-BARD1 in DNA repair and replication, Nat. Rev. Mol. Cell Biol. 21 (5) (2020) 284–299.
[16] W. Zhao, J.B. Steinfeld, F. Liang, X. Chen, D.G. Maranon, C. Jian Ma, Y. Kwon, T. Rao, W. Wang, C. Sheng, X. Song, Y. Deng, J. Jimenez-Sainz, L. Lu, R.B. Jensen, Y. Xiong, G.M. Kupfer, C. Wiese, E.C. Greene, P. Sung, BRCA1-BARD1 promotes RAD51-mediated homologous DNA pairing, Nature 550 (7676) (2017) 360–365.
[17] G. Peng, C. Chun-Jen Lin, W. Mo, H. Dai, Y.Y. Park, S.M. Kim, Y. Peng, Q. Mo, S. Siwko, R. Hu, J.S. Lee, B. Hennessy, S. Hanash, G.B. Mills, S.Y. Lin, Genome-wide transcriptome profiling of homologous recombination DNA repair, Nat. Commun. 5 (2014) 3361.
[18] F. Huang, A.V. Mazin, A small molecule inhibitor of human RAD51 potentiates breast cancer cell killing by therapeutic agents in mouse xenografts, PLoS One 9 (6) (2014), e100993.
[19] X. Jing, F. Yang, C. Shao, K. Wei, M. Xie, H. Shen, Y. Shu, Role of hypoxia in cancer therapy by regulating the tumor microenvironment, Mol. Cancer 18 (1) (2019) 157.
[20] B. Bhattacharya, M.F. Mohd Omar, R. Soong, The Warburg effect and drug resistance, Br. J. Pharmacol. 173 (6) (2016) 970–979.
[21] O. Warburg, On the origin of cancer cells, Science 123 (1956) 309–314.
[22] Y.S. Ko, T. Rugira, H. Jin, Y.N. Joo, H.J. Kim, Radiotherapy-resistant breast cancer cells enhance tumor progression by enhancing premetastatic niche formation through the HIF-1alpha-LOX Axis, Int. J. Mol. Sci. 21 (21) (2020).
[23] J.T. Zhong, Q. Yu, S.H. Zhou, E. Yu, Y.Y. Bao, Z.J. Lu, J. Fan, GLUT-1 siRNA enhances radiosensitization of laryngeal cancer stem cells via enhanced DNA damage, cell cycle redistribution, and promotion of apoptosis in vitro and in vivo, Oncol. Targets Ther. 12 (2019) 9129–9142.
[24] M. Jurikova, L. Danihel, S. Polak, I. Varga, Ki67, PCNA, and MCM proteins: markers of proliferation in the diagnosis of breast cancer, Acta Histochem. 118 (5) (2016) 544–552.
[25] R. Hong, W. Zhang, X. Xia, K. Zhang, Y. Wang, M. Wu, J. Fan, J. Li, W. Xia, F. Xu, J. Chen, S. Wang, Q. Zhan, Preventing BRCA1/ZBRK1 repressor complex binding to the GOT2 promoter results in accelerated aspartate biosynthesis and promotion of cell proliferation, Mol. Oncol. 13 (4) (2019) 959–977.
[26] A. Recht, E.A. Comen, R.E. Fine, G.F. Fleming, P.H. Hardenbergh, A.Y. Ho, C. A. Hudis, E.S. Hwang, J.J. Kirshner, M. Morrow, K.E. Salerno, G.W. Sledge Jr., L. J. Solin, P.A. Spears, T.J. Whelan, M.R. Somerfield, S.B. Edge, Postmastectomy radiotherapy: an American Society of Clinical Oncology, American Society for radiation oncology, and society of surgical oncology focused guideline update, J. Clin. Oncol. 34 (36) (2016) 4431–4442.
[27] M.E.J. Stouthandel, F. Kayser, V. Vakaet, R. Khoury, P. Deseyne, C. Monten, M. Schoepen, V. Remouchamps, A. De Caluwe, G. Janoray, W. De Neve, S. Mazy, L. Veldeman, T. Van Hoof, Delineation guidelines for the lymphatic target volumes in 'prone crawl' radiotherapy treatment position for breast cancer patients, Sci. Rep. 11 (1) (2021) 22529.
[28] Z.R. Zhou, X.Y. Wang, X.L. Yu, X. Mei, X.X. Chen, Q.C. Hu, Z.Z. Yang, X.M. Guo, Building radiation-resistant model in triple-negative breast cancer to screen radioresistance-related molecular markers, Ann. Transl. Med. 8 (4) (2020) 108.
[29] M. Sjöström, D. Lundstedt, L. Hartman, E. Holmberg, F. Killander, A. Kovács, P. Malmström, E. Niméus, E. Werner Rönnerman, M. Fernö, P. Karlsson, Response to radiotherapy after breast-conserving surgery in different breast cancer subtypes in the Swedish breast cancer group 91 radiotherapy randomized clinical trial, J. Clin. Oncol. 35 (28) (2017) 3222–3229.
[30] R. Zhu, W. Li, Y. Xu, J. Wan, Z. Zhang, Upregulation of BTG1 enhances the radiation sensitivity of human breast cancer in vitro and in vivo, Oncol. Rep. 34 (6) (2015) 3017–3024.
[31] P. Gasparini, F. Lovat, M. Fassan, L. Casadei, L. Cascione, N.K. Jacob, S. Carasi, D. Palmieri, S. Costinean, C.L. Shapiro, K. Huebner, C.M. Croce, Protective role of miR-155 in breast cancer through RAD51 targeting impairs homologous recombination after irradiation, Proc. Natl. Acad. Sci. U. S. A. 111 (12) (2014) 4536–4541.
[32] R. Zhong, H. Xu, G. Chen, G. Zhao, Y. Gao, X. Liu, S. Ma, L. Dong, The role of hypoxia-inducible factor-1alpha in radiation-induced autophagic cell death in breast cancer cells, Tumour Biol. 36 (9) (2015) 7077–7083.
[33] R. Ceccaldi, B. Rondinelli, A.D. D'Andrea, Repair pathway choices and consequences at the double-strand break, Trends Cell Biol. 26 (1) (2016) 52–64.
[34] M. Romeo, J.C. Pardo, A. Martinez-Cardus, E. Martinez-Balibrea, V. Quiroga, S. Martinez-Roman, F. Sole, M. Margeli, R. Mesia, Translational research opportunities regarding homologous recombination in ovarian cancer, Int. J. Mol. Sci. 19 (10) (2018).
[35] Y. Zhu, Y. Liu, C. Zhang, J. Chu, Y. Wu, Y. Li, J. Liu, Q. Li, S. Li, Q. Shi, L. Jin, J. Zhao, D. Yin, S. Efroni, F. Su, H. Yao, E. Song, Q. Liu, Tamoxifen-resistant breast cancer cells are resistant to DNA-damaging chemotherapy because of upregulated BARD1 and BRCA1, Nat. Commun. 9 (1) (2018) 1595.
[36] A. Ohmoto, S. Yachida, Current status of poly(ADP-ribose) polymerase inhibitors and future directions, Oncol. Targets Ther. 10 (2017) 5195–5208.
[37] A. Tutt, H. Tovey, M.C.U. Cheang, S. Kernaghan, L. Kilburn, P. Gazinska, J. Owen, J. Abraham, S. Barrett, P. Barrett-Lee, R. Brown, S. Chan, M. Dowsett, J. M. Flanagan, L. Fox, A. Grigoriadis, A. Gutin, C. Harper-Wynne, M.Q. Hatton, K. A. Hoadley, J. Parikh, P. Parker, C.M. Perou, R. Roylance, V. Shah, A. Shaw, I. E. Smith, K.M. Timms, A.M. Wardley, G. Wilson, C. Gillett, J.S. Lanchbury, A. Ashworth, N. Rahman, M. Harries, P. Ellis, S.E. Pinder, J.M. Bliss, Carboplatin in BRCA1/2-mutated and triple-negative breast cancer BRCAness subgroups: the TNT Trial, Nat. Med. 24 (5) (2018) 628–637.
[38] S. Ramachandran, J. Ient, E.L. Gottgens, A.J. Krieg, E.M. Hammond, Epigenetic therapy for solid tumors: highlighting the impact of tumor hypoxia, Genes (Basel) 6 (4) (2015) 935–956.
[39] E.C. de Heer, M. Jalving, A.L. Harris, HIFs, angiogenesis, and metabolism: elusive enemies in breast cancer, J. Clin. Invest. 130 (10) (2020) 5074–5087.
[40] S. Han, J.Y. Choi, Impact of 18F-FDG PET, PET/CT, and PET/MRI on staging and management as an initial staging modality in breast cancer: a systematic review and meta-analysis, Clin. Nucl. Med. 46 (4) (2021) 271–282.
[41] W. Wen, D. Xuan, Y. Hu, X. Li, L. Liu, D. Xu, Prognostic value of maximum standard uptake value, metabolic tumor volume, and total lesion glycolysis of positron emission tomography/computed tomography in patients with breast cancer: a systematic review and meta-analysis, PLoS One 14 (12) (2019), e0225959.
[42] X.F. Li, Y. Du, Y. Ma, G.C. Postel, A.C. Civelek, (18)F-fluorodeoxyglucose uptake and tumor hypoxia: revisit (18)f-fluorodeoxyglucose in oncology application, Transl. Oncol. 7 (2) (2014) 240–247.
[43] V. Bravatà, A. Stefano, F.P. Cammarata, L. Minafra, G. Russo, S. Nicolosi, S. Pulizzi, C. Gelfi, M.C. Gilardi, C. Messa, Genotyping analysis and ^{18}FDG uptake in breast cancer patients: a preliminary research, J. Exp. Clin. Cancer Res. CR 32 (1) (2013) 23.
[44] H.W. Kwon, J.H. Lee, K. Pahk, K.H. Park, S. Kim, Clustering subtypes of breast cancer by combining immunohistochemistry profiles and metabolism

characteristics measured using FDG PET/CT, Cancer imaging: the official publication of the International, Cancer Imaging Soc. 21 (1) (2021) 55.
[45] R. Juliano, M.R. Alam, V. Dixit, H. Kang, Mechanisms and strategies for effective delivery of antisense and siRNA oligonucleotides, Nucleic Acids Res. 36 (12) (2008) 4158–4171.
[46] F. Mercier, J. Paris, G. Kaisin, D. Thonon, J. Flagothier, N. Teller, C. Lemaire, A. Luxen, General method for labeling siRNA by click chemistry with fluorine-18 for the purpose of PET imaging, Bioconjug. Chem. 22 (1) (2011) 108–114.
[47] H. Mukai, K. Hatanaka, N. Yagi, S. Warashina, M. Zouda, M. Takahashi, K. Narushima, H. Yabuuchi, J. Iwano, T. Kuboyama, J. Enokizono, Y. Wada, Y. Watanabe, Pharmacokinetic evaluation of liposomal nanoparticle-encapsulated nucleic acid drug: a combined study of dynamic PET imaging and LC/MS/MS analysis, J. Control Rel. 294 (2019) 185–194.
[48] K. Hatanaka, T. Asai, H. Koide, E. Kenjo, T. Tsuzuku, N. Harada, H. Tsukada, N. Oku, Development of double-stranded siRNA labeling method using positron emitter and its in vivo trafficking analyzed by positron emission tomography, Bioconjug. Chem. 21 (4) (2010) 756–763.